Dalton Transactions

Mechanistic study on reduction of nitric oxide to nitrous oxide using a dicopper complex

Journal:	*Dalton Transactions*
Manuscript ID	DT-COM-01-2022-000275.R1
Article Type:	Communication
Date Submitted by the Author:	05-Mar-2022
Complete List of Authors:	Kametani, Yohei; Kyushu University, Institute for Materials Chemistry and Engineering ABE, Tsukasa; The University of Tokyo, Department of Basic Science, Graduate School of Arts and Sciences Yoshizawa, Kazunari; Kyushu University, Institute for Materials Chemistry and Engineering Shiota, Yoshihito; Kyushu University, Institute for Materials Chemistry and Engineering

COMMUNICATION

Mechanistic study on reduction of nitric oxide to nitrous oxide using a dicopper complex

2642Received 00th January 20xx,
Accepted 00th January 20xx

DOI: 10.1039/x0xx00000x

Yohei Kametani,[a] Tsukasa Abe,[a] Kazunari Yoshizawa[a] and Yoshihito Shiota*[a]

A density functional theory study was carried out to investigate the reduction mechanisms of NO to N_2O using a dicopper complex reported by Zhang and coworkers (*J. Am. Chem. Soc.* 2019, *141*, 10159–10164). The reaction mechanism consists of three steps: N–N bond formation, isomerization of the resultant N_2O_2 moiety, and cleavage of the N–O bond.

The reduction of nitric oxide (NO) to nitrous oxide (N_2O) is important in biological denitrification and in heterogeneous catalytic processes useful for pollution control.[1-3] In biological systems, this reaction is accomplished by NO reductase (NOR) and flavodiiron NO reductase (FNOR), which convert 2 equiv. of NO, two electrons, and two protons into N_2O and water.[3-15] Extensive efforts have been devoted to fully elucidating the corresponding catalytic cycle. On the basis of experimental evidence, NO reduction is widely acknowledged to proceed via a hyponitrite ($N_2O_2^{2-}$) intermediate via N–N bond formation.[16-23] Another useful clue in unraveling the mechanism is a μ-oxo bridged species (*M*–O–*M*), which has been characterized as the resting state of NOR.[24,25] Still, details of the N–N bond formation, N–O bond cleavage, various possible intermediate species, and the exact timing of metal redox shuttling remain elusive.[26-35] Uncovering such details would provide substantial insights for the design of NOR-related therapeutics as well as for improving NOx purification systems.[36-42]

The reduction of NO to N_2O using mono-[43–47] and dicopper[22,48] complexes has been experimentally demonstrated using information obtained from modeling studies. For example, Zhang and co-workers[49] have reported that NO can be activated by the dicopper complex supported by 1,2-bis(di(pyridin-2-yl)methoxy)benzene (**A**). The reaction of **A** with 3 equiv. of NO provides the (μ-oxo)(μ-nitrosyl)dicopper complex and N_2O (Figure 1). Possible reaction mechanisms based on measured kinetics and isolated intermediates have been postulated. Metz[50] used density functional theory (DFT) calculations to theoretically investigate the reduction of NO to N_2O by monocopper complexes.[44-46] However, in the case of dicopper complexes, the literature contains no studies that present a complete mechanism including all intermediates. We were therefore motivated to propose a reaction mechanism using a dicopper model for the reduction of NO. In a reduction of NO to N_2O using a bimetallic complex, the μ-oxo complex is generally considered an intermediate or a product. Therefore, the presumed reaction pathway is that dicopper complex **A** reacts with 2 equiv. of NO to form μ-oxo complex **B**, followed by another NO coordinating to **B** to give the product complex (Figure 1). In the present study, we focus on the reduction of NO to form N_2O and **B**.

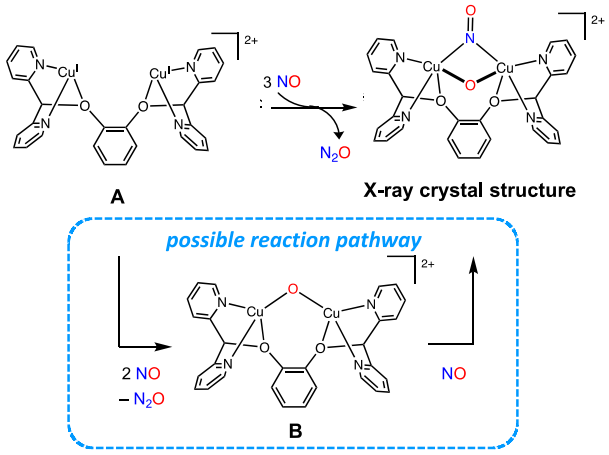

Figure 1 Possible reaction pathway of the NO reduction using dicopper complex **A**.

We here used DFT calculations to investigate how NO reduction occurs via dicopper complex **A**. All calculations were performed using the spin-unrestricted B3LYP functional[51] implemented in the Gaussian 16 package[52] for the structural optimization. Because the total charge of dicopper(I) complex **A** is +2, we considered three possible spin states: closed-shell singlet, open-shell singlet, and triplet states. The open-shell singlet state was computed using the broken-symmetry approach. Vibration frequencies were systematically

[a] *Institute for Materials Chemistry and Engineering and IRCCS, Kyushu University, 744 Motooka, Nishi-ku, Fukuoka, Japan. E-mail: shiota@ms.ifoc.kyushu-u.ac.jp*
Electronic Supplementary Information (ESI) available: [details of any supplementary information available should be included here]. See DOI: 10.1039/x0xx00000x

computed to ensure that the potential energy surface for each optimized geometry corresponded to a local minimum with no imaginary frequencies, or to a saddle point with only one imaginary frequency. We used the (16s10p6d) primitive set of Wachters–Hay supplemented with one polarization *f*-function (α = 1.44 for Cu)[53] for the Cu atoms and the D95** basis set for the H, C, N, and O atoms.[54] We added the Gibbs free energy correction (T = 298.15 K) and the Grimme's dispersion correction (D3).[55] Implicit solvent effects of tetrahydrofuran (ε = 7.4257) were included via the polarizable continuum model (PCM).[56]

Fig. 2 shows calculated free energy profiles for the reduction of NO to N_2O. The calculated reaction mechanism comprises three steps: (1) N–N bond formation (**1**, **TS$_{1/2}$**, **2**); (2) isomerization of the N_2O_2 moiety (**2**, **TS$_{2/3}$**, **3**); and (3) N–O bond cleavage (**3**, **TS$_{3/4}$**, **4**). The DFT calculations suggested that the potential energy surfaces of the closed-shell singlet, open-shell singlet, and triplet states lie close together along the first half of the reaction path. In the first step, the three spin states compete energetically. After formation of the N–N bond, the closed-shell singlet is dominant for the isomerization of the N_2O_2 moiety. In the final step, the open-shell singlet and triplet states are low-lying states. The calculated binding energy between **A** and 2 equiv. of NO is −20.2 kcal/mol to form **1** with the end-on coordination mode. In the triplet state of **1**, the N^a–N^b 1.176 Å, respectively. The N^a–N^b distance of 3.815 Å is too far for the two N atoms to interact. The Cu–Cu distance of 4.454 Å is also too far. The computed spin densities of the Cu atoms in **1 (t)** are nearly zero, and the spin densities are spatially localized at the two NO moieties. Thus, the formal charges of the Cu^a and Cu^b atoms can both be assigned as +1 ($3d^{10}$). Given that the relative energies are –1.0 kcal/mol in the open-shell singlet state and +5.4 kcal/mol in the closed-shell singlet state, the other two spin states in **1** are also energetically possible. The optimized geometry of **1 (oss)** is similar to the triplet geometry, and the N^a–N^b distance is 3.319 Å, whereas **1 (css)** has a short N^a–N^b distance of 1.918 Å. The N^a–N^b bond formation occurs at **TS$_{1/2}$**, which is a transition state. The coordination of the two NO moieties then changes from the end-on mode to the side-on mode, resulting in the formation of the two Cu–O bonds in **2**. The N^a–N^b distance decreases from 1.918 Å in **1** to 1.417 Å in **2** via 1.655 Å in **TS$_{1/2}$** in the closed-shell singlet state. Given the lengths of the N^a–N^b, N^a–O^a, and N^b–O^b bonds, the N_2O_2 moiety of **2** is assigned as the mono-anion $N_2O_2^-$, indicating that one electron was transferred from the dicopper center to the N_2O_2 moiety. The activation energies for **TS$_{1/2}$** are 24.6 kcal/mol in the closed-shell singlet state and 21.8 kcal/mol in the triplet state. Accordingly, the triplet state is dominant to facilitate N–N bond formation.

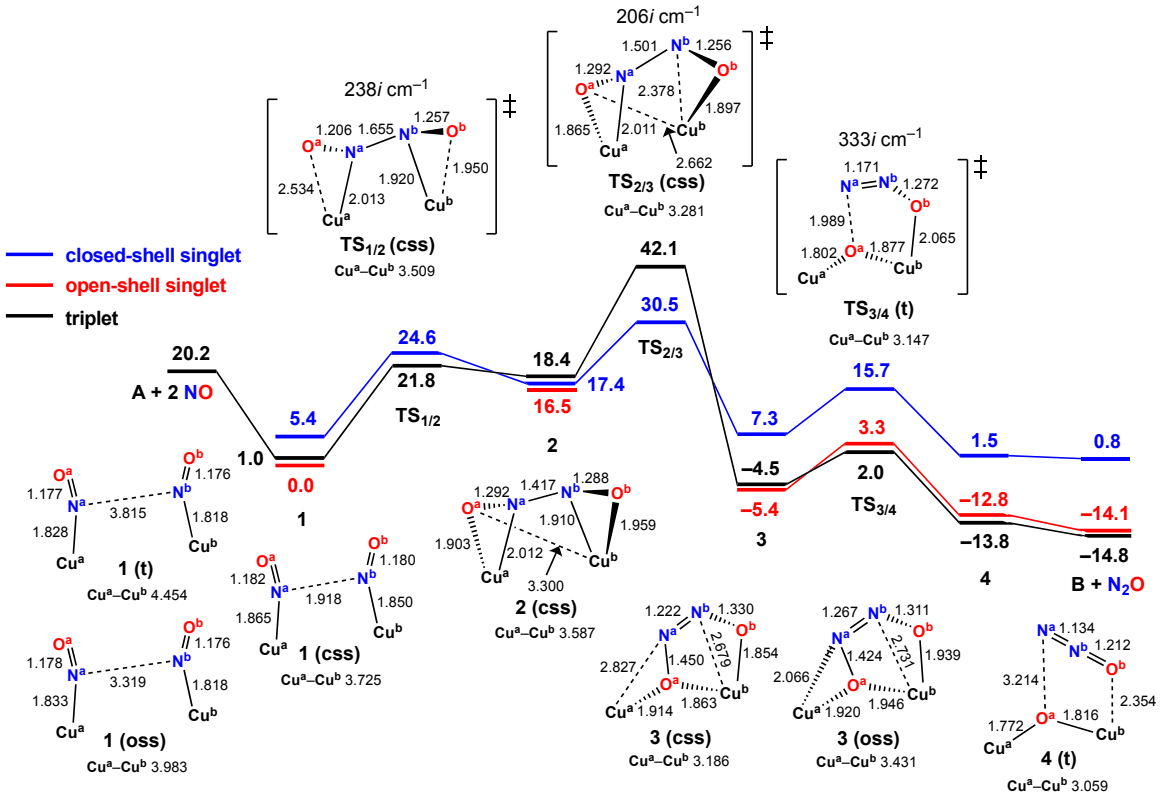

Fig. 2 Gibbs free energy profiles for the reduction of NO to N_2O starting from the dissociation limit of **A** + 2 NO in the closed-shell singlet (blue), open-shell singlet (red) and triplet states (black). Notations, **css**, **oss** and **t**, represent the closed-shell singlet, open-shell singlet and triplet states, respectively. Energies and distances are given in units of kcal/mol and Å, respectively.

O^a and N^b–O^b bond lengths were calculated to be 1.177 Å and

Next, the N_2O_2 moiety of **2** isomerizes via **$TS_{2/3}$**, which is a transition state corresponding to the cleavage of the Cu^b–N^b bond and the formation of the Cu^b–O^a bond. In the closed-shell singlet state, the Cu^b–N^b bond distance increases from 1.910 Å in **2** to 2.679 Å in **3** via 2.378 Å in **$TS_{2/3}$**, whereas the Cu^b–O^a bond distance decreases from 3.300 Å in **2** to 1.946 Å in **3** via 2.662 Å in **$TS_{2/3}$**. This step also corresponds to the *cis*–*trans* isomerization with respect to the O^a–N^a–N^b–O^b dihedral angle, which decreases from 154.4° in **2** to 3.6° in **3** via 75.8° in **$TS_{2/3}$**. Calculated energies of **$TS_{2/3}$** are 42.1 kcal/mol in the triplet state and 30.5 kcal/mol in the closed-shell singlet state. Thus, the singlet pathway is energetically favored, leading to the formation of **3**. The DFT calculations indicate that electron transfer occurs from the Cu center to the N_2O_2 moiety. In fact, the N^a–N^b bond distance decreases from 1.344 Å in **2** to 1.267 Å in **3** via 1.501 Å in **$TS_{2/3}$**. The N^a–N^b bond is shortened during the step from **2** to **3**, whereas it is elongated in the vicinity of **$TS_{2/3}$**. Such a change of the N^a–N^b bond length represents a decrease in the π-character of the N^a–N^b bond, which facilitates the *trans*–*cis* rotation. After **$TS_{2/3}$**, the ground state of **3** changes from the closed-shell singlet to the triplet state.

To help the better understanding of the change in the electronic state induced by the isomerization, we performed an orbital analysis. Figure 3 shows (a) schematic representation electronic states from **2** to **3** and (b) an orbital analysis of the isolate N_2O_2 molecule with the dihedral angle of 75.8˚ and **$TS_{2/3}$ (css)**. The N_2O_2 moiety was assigned to mono anion in **2**, neutral molecule in **$TS_{2/3}$** and dianion in **3** from geometrical information of N_2O_2 species (SI). The orbital analysis of **$TS_{2/3}$** shows that the occupied orbital of **$TS_{2/3}$** has the same σ(N-N) orbital as the neutral N_2O_2 molecule. Furthermore, similarities were observed for other orbitals, indicating that **$TS_{2/3}$** and the neutral N_2O_2 molecule have a similar electronic configuration. Thus, our DFT calculations suggest that the valence of the dicopper active site changes from Cu(I)Cu(II) in **2** to Cu(II)Cu(II) or Cu(I)Cu(III) in **3** via Cu(I)Cu(I) in **$TS_{2/3}$**. The orbital analysis of **$TS_{2/3}$** is also consistent with the ground singlet state.

The closed-shell singlet state and the open-shell singlet state of **3** correspond to Cu(I)Cu(III) and Cu(II)Cu(II), respectively. The disproportionate valence of Cu^a and Cu^b is energetically unfavorable for **3**; thus, one electron is transferred to form the open-shell singlet state of the two Cu(II) centers. The geometrical structure of **3** is unique, where the N_2O_2 moiety coordinates to the two Cu ions to form a μ-oxo structure. On the basis of the Mulliken spin densities, we assigned the formal charges of the Cu^a and Cu^b atoms and the N_2O_2 moiety in **3 (oss), (t)** as +2, +2, and −2, respectively. Notably, the N^a–O^a bond of **3** is distinctively elongated to 1.424 Å in **3 (oss)**, which is longer than the N–O bond of the *cis*-$N_2O_2^{2-}$ dianion (calculated to be 1.362 Å). A similar intermediate has been reported in the NO reduction by a diiron complex, which is a model of FNOR.[57]

In the final step, N^a–O^a bond cleavage occurs to provide the (μ-oxo)dicopper(II) complex and an N_2O molecule. During the N^a–O^a bond cleavage, the N^a–N^b and N^b–O^b bonds shorten and the N^a–N^b–O^b geometry changes from bent to linear. In addition, the Cu–Cu distance is further shortened (3.059 Å in **4 (t)**) to form a μ-oxo bridge. The open-shell singlet and triplet states are dominant in this step because **$TS_{3/4}$ (oss)** and **$TS_{3/4}$ (t)** are lower in energy by 12.4 and 13.7 kcal/mol than **$TS_{3/4}$ (css)**, respectively. The activation energies of **$TS_{3/4}$** are 6.5 kcal/mol in the triplet state and 8.7 kcal/mol in the open-shell singlet state. In the N^a–O^a bond cleavage, the Mulliken charges of the two Cu atoms remain unchanged. The charge of the O^a atom decreases from −0.40 to −0.59, whereas the total charges of the N^a, N^b, and O^b atoms increase from –0.17 to 0.12. Therefore, this step is completed by the electron transfer from the N^a, N^b, and O^b atoms to the O^a atom. In **4**, the open-shell singlet and triplet states are stable and no significant differences in geometry or energy are observed. The spin density of the N_2O moiety is almost zero. Accordingly, the $N^aN^bO^b$ moiety exists as the N_2O molecule, indicating that little interaction occurs between the (μ-oxo)dicopper complex and the N_2O molecule. Finally, the desorption energy of N_2O from **4** requires 7.4 kcal/mol (electronic energy) to give the (μ-oxo)dicopper complex **B** in the triplet state. However, the desorption energy becomes unnecessary when entropy correction is considered, as shown in Figure 2.

We next consider the small activation energy for the cleavage of the N–O bond in **3**. We have reported a reaction mechanism for NO reduction in which protonation of the NO

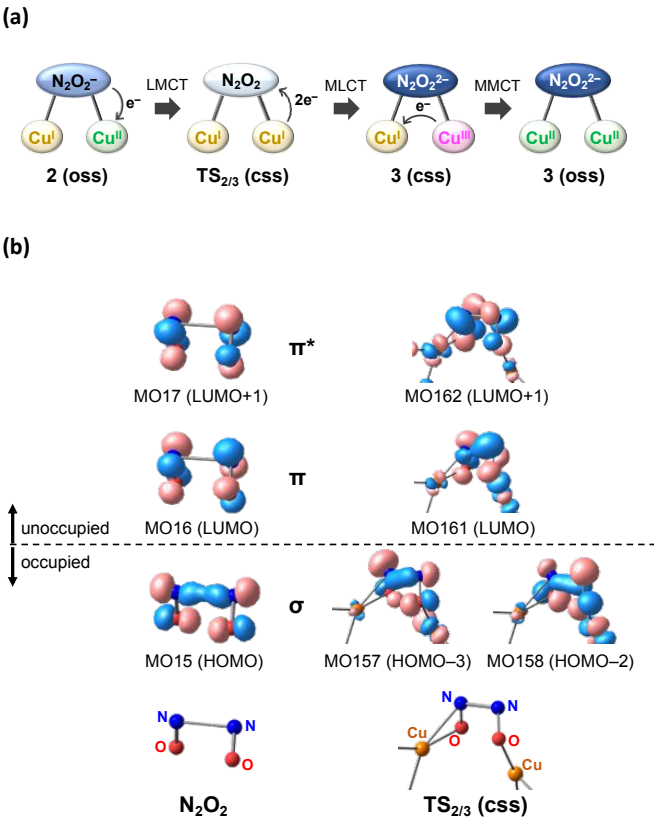

Figure 3. (a) Schematic representation of electronic states from **2** to **3**. (b) Molecular orbitals of N_2O_2 molecule and **$TS_{2/3}$ (css)**. The N_2O_2 molecule was produced by rotating the O–N–N–O dihedral angle of the optimized *cis*-N_2O_2 molecule to 75.8°.

moiety facilitates the formation of N–N bonds;[58,59] however, the cleavage of the N–O bond in the N_2O formation process requires a large activation energy and the mechanism by which it proceeds energetically favorably remains unclear. For example, in the NO reduction by copper-exchanged zeolite (Cu-ZSM-5),[58] an O–N=N–O intermediate corresponding to **3** has an N–O bond length of 1.230 Å and the activation energy for cleavage of the N–O bond is 55.3 kcal/mol. In the NO reduction by a diruthenium complex,[59] the intermediate has an N–O bond length of 1.344 Å and the activation energy is 17.4 kcal/mol.[59] By contrast, the N^a–O^a bond is elongated to 1.424 Å and cleavage of the N–O bond can occur with an activation energy of only 8.7 kcal/mol. In dicopper complex **3**, the N^a–O^a and N^b–O^b bonds have different lengths of 1.424 Å and 1.311 Å, respectively. In particular, the N^aO^a moiety is coordinated to the two Cu atoms as [Cu^a–(μ-η^2:η^1-N^aO^a)–Cu^b], whereas the N^bO^b is coordinated end-on to one Cu atom [Cu^b–O^bN^b]. From the structural analysis, this unusual coordination to Cu plays an important role in the N–O bond cleavage in the final step.

Conclusions

We have investigated the mechanism for the reduction of NO to N_2O by a dicopper complex using DFT calculations. The computed results indicate that the reaction consists of three fundamental steps: (1) N–N bond formation, (2) isomerization of the N_2O_2 moiety and (3) N–O bond cleavage. The calculated reaction mechanism predicts that the coupling of two NO molecules initially occurs. The two NO molecules then transform from the end-on to the side-on mode. The first step requires an activation energy of 21.8 kcal/mol in the triplet state and is the rate-determining step in this mechanism. The *cis*–*trans* isomerization of the N_2O_2 moiety then occurs as the O atom is bridged between two Cu atoms with an activation energy of 13.1 kcal/mol in the closed-shell singlet state. Finally, cleavage of the N–O bond occurs to give $[Cu_2(\mu\text{-O})]^{2+}$ with N_2O. The elongated N–O bond in the reaction intermediate $[Cu_2(\mu\text{-ONNO})]^{2+}$ contributes to the small activation energy of only 6.5 kcal/mol in the triplet state. The overall reaction was calculated to be exothermic by 35.0 kcal/mol in the triplet state. These computed results are consistent with the experimental observation, where N_2O is released using the dicopper complex. In addition, the large binding energy of NO and Cu atoms in the reactant complex $[Cu_2(NO)_2]^{2+}$ and the small binding energy of N_2O in the product complex $[Cu_2(N_2O)(\mu\text{-O})]^{2+}$ favor this catalytic cycle.

Conflicts of interest

There are no conflicts to declare.

Acknowledgements

K. Y. acknowledges KAKENHI Grant numbers JP15K13710, JP17H03117 and JP20H05671 from the Japan Society for the Promotion of Science (JSPS) and the Ministry of Education, Culture, Sports, Science and Technology of Japan (MEXT), the MEXT Projects of “Integrated Research Consortium on Chemical Sciences”, “Cooperative Research Program of Network Joint Research Center for Materials and Devices”, “Elements Strategy Initiative to Form Core Research Center”, JST-CREST JPMJCR15P5 and JST-Mirai JPMJMI18A2. The computational study was mainly carried out using the computer facilities at Research Institute for Information Technology, Kyushu University.

References

1 C. Ferousi, S. H. Majer, I. M. DiMucci and K. M. Lancaster, *Chem. Rev.*, 2020, **120**, 5252–5307.
2 P. Granger and V. I. Parvulescu, *Chem. Rev.*, 2011, **111**, 3155–3207.
3 I. M. Wasser, S. Vries, P. Moënne-Loccoz, I. Schröder and K. D. Karlin, *Chem. Rev.*, 2002, **102**, 1201–1234.
4 J. Wang, M. P. Schopfer, S. C. Puiu, A. A. N. Sarjeant and K. D. Karlin, *Inorg. Chem.*, 2010, **49**, 1404–1419.
5 T. Hayashi, J. D. Caranto, D. A. Wampler, D. M. Kurtz, Jr. andP. Moënne-Loccoz, *Biochemistry*, 2010, **49**, 7040—7049.
6 T. Hayashi, J. D. Caranto, H. Matsumura, D. M. Kurtz, Jr. andP. Moënne-Loccoz, *J. Am. Chem. Soc.*, 2012, **134**, 6878–6884.
7 D. M. Kurtz, Jr., *Dalton Trans.*, 2007, 4115–4121.
8 R. Silaghi-Dumitrescu, E. D. Coulter, A. Das, L. G. Ljungdahl, G. N. L. Jameson, B. H. Huynh and D. M. Kurtz, Jr., *Biochemistry*, 2003, **42**, 2806–2815.
9 M. P. Schopfer, J. Wang and K. D. Karlin, *Inorg. Chem.*, 2010, **49**, 6267–6282.
10 J. Wang, M. P. Schopfer, A. A. N. Sarjeant and K. D. Karlin, *J. Am. Chem. Soc.*, 2009, **131**, 450–451.
11 T. D. Ju, A. S. Woods, R. J. Cotter, P. Moënne-Loccoz and K. D. Karlin, *Inorg. Chim. Acta*, 2000, **297**, 362–372.
12 J. P. Collman, Y. Yang, A. Dey, R. A. Decraeau, S. Ghosh, T. Ohta and E. I. Solomon, *Proc. Natl. Acad. Sci. U.S.A.*, 2008, **105**, 15660–15665.
13 J. P. Collman, A. Dey, Y. Yang, R. A. Decraeau, T. Ohta and E. I. Solomon, *J. Am. Chem. Soc.*, 2008, **130**, 16498–16499.
14 J. P. Collman, Y.-L. Yan, J. Lei and P. H. Dinolfo, *Inorg. Chem.*, 2006, **45**, 7581–7583.
15 S. Zheng, T. C. Berto, E. W. Dahl, M. B. Hoffman, A. L. Speelman and N. Lehnert, *J. Am. Chem. Soc.*, 2013, **135**, 4902–4905.
16 W. A. Brown, P. Gardner and D. A. King, *J. Phys. Chem.*, 1995, **99**, 7065–7074.
17 W. A. Brown and D. A. King, *J. Phys. Chem. B*, 2000, **104**, 2578–2595.
18 A. Shiotari, Y. Kitaguchi, H. Okuyama, S. Hatta and T. Aruga, *Phys. Rev. Lett.*, 2011, **106**, 156104.
19 A. Shiotari, S. Hatta, H. Okuyama and T. Aruga, *J. Chem. Phys.*, 2014, **141**, 134705.
20 C. Hess, E. Ozensoy, C.-W. Yi and D. W. Goodman, *J. Am. Chem. Soc.*, 2006, **128**, 2988– 2994.
21 C. Varotsis, T. Ohta, T. Kitagawa, T. Soulimane and E. Pinakoulaki, *Angew. Chem. Int. Ed.*, 2007, **46**, 2210–2214.
22 G. B. Wijeratne, S. Hematian, M. A. Siegler and K. D. Karlin, *J. Am. Chem. Soc.*, 2017, **139**, 13276–13279.
23 G. B. Wijeratne, M. Bhadra, M. A. Siegler and K. D. Karlin, *J. Am. Chem. Soc.*, 2019, **141**, 17962–17967.
24 P. Girsch, *Biochim. Biophys. Acta*, 1997, **1318**, 202-216.
25 P. Moënne-Loccoz, *J. Am. Chem. Soc.*, 1998, **120**, 5147-5152.
26 C. K. Brozek, J. T. Miller, S. A. Stoian and M. Dincă, *J. Am. Chem. Soc.*, 2015, **137**, 7495–7501.

27 G. A. Poskrebyshev, V. Shafirovich and S. V. Lymar, *J. Am. Chem. Soc.*, 2004, **126**, 891–899.
28 T. Ohta, T. Soulimane, T. Kitagawa and C. Varotsis, *Phys. Chem. Chem. Phys.*, 2015, **17**, 10894–10898.
29 Y. Arikawa, T. Asayama, Y. Moriguchi, S. Agari and M. Onishi, *J. Am. Chem. Soc.*, 2007, **129**, 14160−14161.
30 J. D. Caranto, A. Weitz, M. P. Hendrich and D. M. Kurtz, Jr., *J. Am. Chem. Soc.*, 2014, **136**, 7981–7992.
31 J. Yi, B. H. Morrow, A. L. O. C. Campbell, J. K. Shen and G. B. Richter-Addo, *Chem. Commun.*, 2012, **48**, 9041–9043.
32 M. R. A. Blomberg, *Biochemistry*, 2017, **56**, 120–131.
33 T. C. Berto, A. L. Speelman, S. Zheng and N. Lehnert, *Coord. Chem. Rev.*, 2013, **257**, 244–259.
34 S. Chakraborty, J. Reed, M. Ross, M. J. Nilges, I. D. Petrik, S. Ghosh, S. Hammes-Schiffer, J. T. Sage, Y. Zhang, C. E. Schulz and Y. Lu, *Angew. Chem., Int. Ed.*, 2014, **53**, 2417–2421.
35 S. Sabuncu, J. H. Reed, Y. Lu and P. Moënne-Loccoz, *J. Am. Chem. Soc.*, 2018, **140**, 17389–17393.
36 K. Kakishima, A. Shiratsuchi, A. Taoka, Y. Nakanishi and Y. Fukumori, *Biochem. Biophys. Res. Commun.*, 2007, **355**, 587–591.
37 M. C. Justino, C. Ecobichon, A. F. Fernandes, I. G. Boneca and L. M. Saraiva, *Antioxid. Redox Signaling*, 2012, **17**, 1190–1200.
38 A. Flint, A. Stintzi and L. M. Saraiva, *FEMS Microbiol. Rev.*, 2016, **40**, 938–960.
39 A. P. Gobert and K. T. Wilson, *Trends Microbiol.*, 2016, **24**, 366–376.
40 A. Vázquez-Torres, A. J. Bäumler, *Curr. Opin. Microbiol.*, 2016, **29**, 1–8.
41 A. R. Ravishankara, J. S. Daniel and R. W. Portmann, *Science*, 2009, **326**, 123–125.
42 R. de Richter and S. Caillol, *J. Photochem. Photobiol., C*, 2011, **12**, 1–19.
43 W. B. Tolman, *Inorg. Chem.*, 1991, **30**, 4877–4880.
44 C. E. Ruggiero, S. M. Carrier, W. E. Antholine, J. W. Whittaker, C. J. Cramer and W. B. Tolman, *J. Am. Chem. Soc.*, 1993, **115**, 11285–11298.
45 C. E. Ruggiero, S. M. Carrier and W. B. Tolman, *Angew. Chem., Int. Ed.*, 1994, **33**, 895–897.
46 J. L. Schneider, S. M. Carrier, C. E. Ruggiero, V. G. Young, Jr. and W. B. Tolman, *J. Am. Chem. Soc.*, 1998, **120**, 11408–11418.
47 S. Kim, M. A. Siegler and K. D. Karlin, *Chem. Commun.*, 2014, **50**, 2844–2846.
48 P. P. Paul and K. D. Karlin, *J. Am. Chem. Soc.*, 1991, **113**, 6331–6332.
49 W. Tao, J. K. Bower, C. E. Moore and S. Zhang, *J. Am. Chem. Soc.*, 2019, **141**, 10159–10164.
50 S. Metz, *Inorg. Chem.*, 2017, **56**, 3820–3833.
51 A. D. Becke, *Phys. Rev. A*, 1988, **38**, 3098–3100; C. Lee, W. Yang and R. G. Parr, *Phys. Rev. B*: *Condens. Matter Mater. Phys.*, 1988, **37**, 785–789; A. D. Becke, *J. Chem. Phys.*, 1993, **98**, 5648–5652.
52 M. J. Frisch et al. *Gaussian 16*, *Revision A. 03*; Gaussian, Inc.: Wallingford, CT, 2016.
53 A. J. H. Wachters, *J. Chem. Phys.*, 1970, **52**, 1033–1036; P. J. Hay, *J. Chem. Phys.*, 1977, **66**, 4377–4384; K. Raghavachari and G. W. Trucks, *J. Chem. Phys.*, 1989, **91**, 1062–1065.
54 T. H. Dunning and P. J. Hay, in *Modern Theoretical Chemistry*, ed. H. F. Schaefer III, Plenum, New York, 1976, vol. 3, pp. 1–27.
55 T. Schwabe and S. Grimme, *Phys. Chem. Chem. Phys.*, 2007, **9**, 3397–3406; S. Grimme, J. Antony, S. Ehrlich and H. Krieg, *J. Chem. Phys.*, 2010, **132**, 154104–154119.
56 J. Tomasi, B. Mennucci and R. Cammi, *Chem. Rev.*, 2005, **105**, 2999–3093.
57 C. Van Stappen and N. Lehnert, *Inorg. Chem.*, 2018, **57**, 4252–4269.
58 P. K. Sajith, Y. Shiota, and K. Yoshizawa, *ACS Catal.*, 2014, **4**, 2075–2085.
59 T. Suzuki, H. Tanaka, Y. Shiota, P. K. Sajith, Y. Arikawa and K. Yoshizawa, *Inorg. Chem.*, 2015, **54**, 7181–7191.